

Mid-Miocene climatic optimum: Clay mineral evidence from the red clay succession, Longzhong Basin, Northern China

Yongui Song^{a,e,*}, Qiansuo Wang^{b,c,**}, Zhisheng An^a, Xiaoke Qiang^a, Jibao Dong^a, Hong Chang^a, Maosheng Zhang^d, Xiaohua Guo^e

^a State Key Laboratory of Loess and Quaternary Geology, Institute of Earth Environment, Chinese Academy of Sciences, Xi'an 710061, China

^b Shandong Provincial Key Laboratory of Water and Soil Conservation and Environmental Protection, College of Resources and Environment, Linyi University, Linyi 276000, China

^c Key Laboratory of Virtual Geographic Environment, Ministry of Education, Nanjing Normal University, Nanjing 210023, China

^d Key Laboratory for Geo-hazard in Loess Area, Xi'an Centre of Geological Survey, Geological Survey of China, Xi'an 710054, China

^e Department of Geosciences, Baylor University, Waco, TX 76798, USA



ARTICLE INFO

Keywords:

X-ray diffraction
Geochemistry
Miocene climate
Global warming event
Tibetan Plateau

ABSTRACT

The Mid-Miocene Climatic Optimum (MMCO) is one of Earth's most recent prolonged warming events, recorded in both the deep ocean and mid- to high-latitude continents. Thick Cenozoic deposits in the Longzhong Basin, Northwest China, provide great potential for characterizing the MMCO, but have not been well documented. In this study, we carry out clay mineralogical and geochemical analyses of the Miocene red clay succession from the eastern Longzhong Basin, employing X-ray diffraction and geochemistry, and discuss the climatic characteristics of the MMCO. The results reveal that the MMCO occurred at 16–14 Ma and is associated with relatively high kaolinite and smectite contents, high illite crystallinity values and kaolinite/(illite + chlorite) ratio, and lower chlorite and illite contents. These clay mineral assemblages confirm a warm and moist climate during the MMCO. Furthermore, the $\text{SiO}_2/\text{Al}_2\text{O}_3$ ratio declined with increasing Al_2O_3 , indicative of greater precipitation and intensified weathering during this period. When compared with local and global records, we find that our clay mineral records reflect regional climatic change superimposed upon global climatic trends during the MMCO. It is suggested that a high concentration of CO_2 , and associated global warming, may have been responsible for the MMCO, rather than the uplift of the Tibetan Plateau.

1. Introduction

The global climate underwent significant change during the Cenozoic era, shifting from a warm, ice-free climate to a cold climate marked by the massive continental ice sheets (Zachos et al., 2001). This era witnessed the last global climate optimum, referred to as the Mid-Miocene Climate Optimum (MMCO), which may have occurred at 16–14.8 Ma (Flower and Kennett, 1994), 17–15 Ma (Böhme, 2003; Wan et al., 2009; Zachos et al., 2001) or 18–15 Ma (Sun and Zhang, 2008). The MMCO represents a geologically recent warming event unrelated to human activity that may provide an analog for future global warming (Böhme, 2003; Goldner et al., 2014; Pierce et al., 2017; Sun and Zhang, 2008; You et al., 2009; Zachos et al., 2001; Zan et al., 2015; Zhao et al., 2017). The MMCO was characterized by a mid-latitude warming of ca. 6 °C relative to present, beginning with an extended period of global

warmth and ending with the development of permanent ice sheets in Antarctica, thus marking one of the four major steps in Cenozoic cooling (Böhme, 2003; Harzhauser et al., 2011; Hui et al., 2011; Lewis et al., 2007; Miller et al., 1991; Sun and Zhang, 2008; Zan et al., 2015). After the MMCO, an abrupt cooling occurred in the middle and high latitudes, and the average global temperature dropped > 5 °C as the East Antarctic Ice Sheet developed, during a process known as the Mid-Miocene Climatic Cooling (MMCC) (Flower and Kennett, 1994; George et al., 2001; Holbourn et al., 2013; Larsson et al., 2011; Lewis et al., 2008; Turco et al., 2001). Until now, the MMCO and MMCC events have mostly been reconstructed using oxygen isotope records from deep-sea sediments. In contrast to marine sediments, evidence of the MMCO in terrestrial sediments remains relatively scarce because of the depositional hiatuses (Sun and Zhang, 2008). It is difficult to find a single, continuous sequence of deposits covering the entire Cenozoic.

* Correspondence to: Y.G. Song, State Key Laboratory of Loess and Quaternary Geology, Institute of Earth Environment, Chinese Academy of Sciences, Xi'an 710061, China.

** Correspondence to: Q.S. Wang, Shandong Provincial Key Laboratory of Water and Soil Conservation and Environmental Protection, College of Resources and Environment, Linyi University, Linyi 276000, China.

E-mail addresses: syg@ieecas.cn (Y. Song), wangqiansuo@lyu.edu.cn (Q. Wang).

<http://dx.doi.org/10.1016/j.palaeo.2017.10.001>

Received 5 June 2017; Received in revised form 25 September 2017; Accepted 1 October 2017

Available online 02 October 2017

0031-0182/ © 2017 Elsevier B.V. All rights reserved.

Few attempts have been made to identify the MMCO event, its timing and climatic characteristics, and the possible driving mechanisms during this period in Northern China remain poorly understood (Miao et al., 2011; Sun and Zhang, 2008; Sun et al., 2015; Zhao et al., 2017). Thick Cenozoic deposits such as those in the Longzhong Basin in Northern China not only provide great potential for understanding the tectonic history and paleoclimatic changes (Alonso-Zarza et al., 2009; Dupont-Nivet et al., 2007; Fang et al., 2003; Miao et al., 2011; W. Wang et al., 2016; Zhang et al., 2014), but also give us new insights into the evolution and driving mechanisms of the MMCO. Since the discovery of 22 Ma (Guo et al., 2002) or 25 Ma (Qiang et al., 2011) of eolian sediments in the Longzhong Basin, much attention has been paid to their genesis (Alonso-Zarza et al., 2009; Guo et al., 2010), their implications for Asian desertification (Guo et al., 2002; Qiang et al., 2011; Zhang et al., 2015) and tectonic change (Fang et al., 2003; Liu et al., 2015; W. Wang et al., 2016). A 654 m core of red clay spanning 25.6 to 4.8 Ma from Zhuanglang (ZL) in the eastern margin of the Longzhong Basin (Qiang et al., 2011) provides an opportunity to explore the MMCO.

Clay mineral analysis is one of the important tools for reconstructing paleoclimatic changes over different timescales (Kemp et al., 2016; Liu et al., 2003; Moore and Reynolds, 1997; Thiry, 2000; Xu et al., 2017). Previous studies (Gao et al., 2013; Gylesjö and Arnold, 2006; Hong et al., 2017; Hong et al., 2010; Liu et al., 2010; Liu et al., 2003; Pal et al., 2012; Song et al., 2014) have indicated that paleoclimatic records obtained from clay minerals agree well with those obtained by other proxies in the continental and ocean deposits. For example, clay mineral assemblages have been successfully used to investigate climatic transition events such as the Eocene-Oligocene climatic transition in the Xining Basin (Zhang and Guo, 2014) and Tarim Basin (Wang et al., 2013), the early-Eocene Climate Optimum (EECO) event in the Qaidam Basin (C. Wang et al., 2011) and an early-Pliocene warmer and wetter event in the Qinghai Lake Basin (Zeng et al., 2014). In this study, we attempt to reconstruct paleoclimatic evolution and the driving forces during the MMCO period, on the basis of clay mineralogy of eolian sediments in the Longzhong Basin.

2. Geological setting and stratigraphy

The Longzhong Basin is situated in the transition zone between the Chinese Loess Plateau and Northeastern Tibetan Plateau, and is surrounded by the Liupan Mountains, West Qinling Mountains and Qilian Mountains (Fig. 1A). It is composed of several sub-basins: from west to east, these are the Xining Basin, Lanzhou Basin, Linxia Basin and Longxi-Jingning Basin, each containing thick Cenozoic deposits unconformably overlying the pre-Cenozoic stratigraphy (Li et al., 2006; Qu and Cai, 1984; X. Wang et al., 2011; Z. Wang et al., 2016). The Cenozoic succession in the Longzhong basin can be classified into the Paleogene Guyuan Group and the Neogene Gansu Group on the basis of lithofacies and paleontology (Qu and Cai, 1984). The Paleogene Guyuan Group is mainly present in the Xining, Lanzhou and Linxia sub-basins and at the southern edge of the Longzhong Basin (Fig. 1A), and is characterized by massive conglomerates and sandstones with thicknesses varying from several tens to hundreds of meters (Qu and Cai, 1984; Wang et al., 2012; X. Wang et al., 2011; Z. Wang et al., 2016). The Neogene Gansu Group contains different kinds of sediments, including the eolian red clay-paleosol succession, reworked loess, fluvial and lacustrine deposits. The aqueous deposits are mainly composed of fluvial sandstone, lacustrine marl, and flood plain mudstone with abundant mammal fossils (Alonso-Zarza et al., 2009; Ao et al., 2016; Li et al., 2006). The Gansu Group is primarily distributed in the depression belt and the intermontane basins. The typical eolian red clay succession, spanning 25–3.5 Ma, is widely deposited on the bedrock platforms and basin margins of the highlands (Fig. 1B) (Guo et al., 2002; Z. Wang et al., 2016; Zhan et al., 2010). The characteristics of these Cenozoic sediments are sensitive to the uplift of the Tibetan Plateau, East Asia monsoon evolution, and inland Asian aridification (Dupont-Nivet et al.,

2007; Guo et al., 2002; Li et al., 2006; Liang et al., 2014; Liu et al., 2015; Wang et al., 2012; W. Wang et al., 2016; Z. Wang et al., 2016; Xiao et al., 2012; Zhang et al., 2016).

The Zhuanglang (ZL) drilling site (35°13'N, 106°05'E) is located at the eastern margin of the Longxi-Jingning sub-basin in the Longzhong Basin, near the west piedmont of the Liupan Mts (Fig. 1A, B). The site lies about 60 km northeast of the famous Miocene loess-soil sequence QAI-II section (Guo et al., 2002), 30 km from the QAI-III section (Hao and Guo, 2007), and 70 km north of the aqueous deposits in the Yaodian (YD) section (Alonso-Zarza et al., 2009; Li et al., 2006) (Fig. 1B). The ZL drilling core was combined from two parallel drilling sites, and has a composite length of 654 m (Qiang et al., 2011). The core is mainly composed of the Neogene Gansu Group with an eolian red clay-paleosol sequence. Detailed magnetostratigraphic correlations indicated that the ZL core sequence spanned from 25.6 to 4.8 Ma (Fig. 2) (Qiang et al., 2011). The composite ZL core can be divided into 5 lithologic units, which are described as follows (Fig. 2). Unit V is Oligocene purplish-red to light-brown sandy gravels interbedded with thin red clay; Unit IV (584.7–628.3 m, 23.6–25 Ma) is red clay and sand/gravel layers, in which the red clay has a clear aggregate-like silty structure with carbonate nodules and dark coatings; Unit III (124.3–584.7 m, 8.1–23.6 Ma) is alternate yellowish brown loess/weakly developed paleosols and reddish brown paleosol horizons; Unit II (3.3–124.3 m, 4.8–8.1 Ma) consists of red clay intercalated with yellowish-brown to greyish-brown sand and gravel; Unit I (0–3.3 m) is yellowish Late Pleistocene Malan loess. The Cenozoic sediments rest unconformably on the Proterozoic dark grey biotite gneiss (Fig. 2). Magnetic susceptibility has notably high values at 16–14 Ma (Qiang et al., 2011; Zhao et al., 2017), but the grain size (Sun et al., 2015), and color and structure of the sediments (Fig. 2) show no obvious changes during the middle Miocene. According to the magnetostratigraphy and magnetic susceptibility variations of the ZL core, we chose 80 samples at depths from 240 m (12 Ma) to 390 m (17 Ma) for clay mineral analysis (Fig. 2).

3. Methods

The isolation of < 2 µm clay fractions was followed by the Chinese oil and gas industry standard analysis SY/T 5163-2010 (NEA, 2010). The clay fraction was separated by sedimentation and centrifugation. The dry samples were treated with dilute HCl to remove the calcium carbonate and H₂O₂ to remove organic matter; the clay fractions were separated by gravity separation using Stoke's Law determinations. Then, clay was separated by centrifugation in deionized water to remove free ions. The scraping slide technique (Liu et al., 2004, 2003; Zeng et al., 2014) was used to prepare oriented mounts. In order to identify and quantify the clay minerals present, X-ray diffraction (XRD) analysis of the oriented mounts was carried out for each sample under natural (air-dried) conditions (N), ethylene-glycol solvation for 24 h in a desiccator (EG), and heating at 550 °C for 2 h (H). XRD patterns were obtained using a PANalytical X'Pert Pro MPD diffractometer with CuKα radiation and Ni filter, under a voltage of 40 kV and a current of 40 mA. Scans were performed from 3° to 30°, with a step size of 0.0167°. Next, a high-resolution scan from 24° to 26° 2θ at a rate of 0.1° 2θ per minute was performed to isolate the contributions of kaolinite and chlorite in the 3.5 Å peak. The ratio of kaolinite to chlorite was calculated from the peak areas of 3.58 Å and 3.53 Å. Identification of clay minerals was based primarily on the position of the (001) series of basal reflections in the three diagnostic XRD patterns.

Semi-quantitative estimates of clay minerals were determined from the basal reflection peak areas: these comprised smectite (17 Å) (including random illite/smectite mixed-layers), illite (10 Å), and kaolinite/chlorite (7 Å) on the ethylene-glycol diffraction traces (Moore and Reynolds, 1997) using MacDiff 4.2.6 software (Petschick, 2000). The relative abundances of clay minerals were determined using the formula:

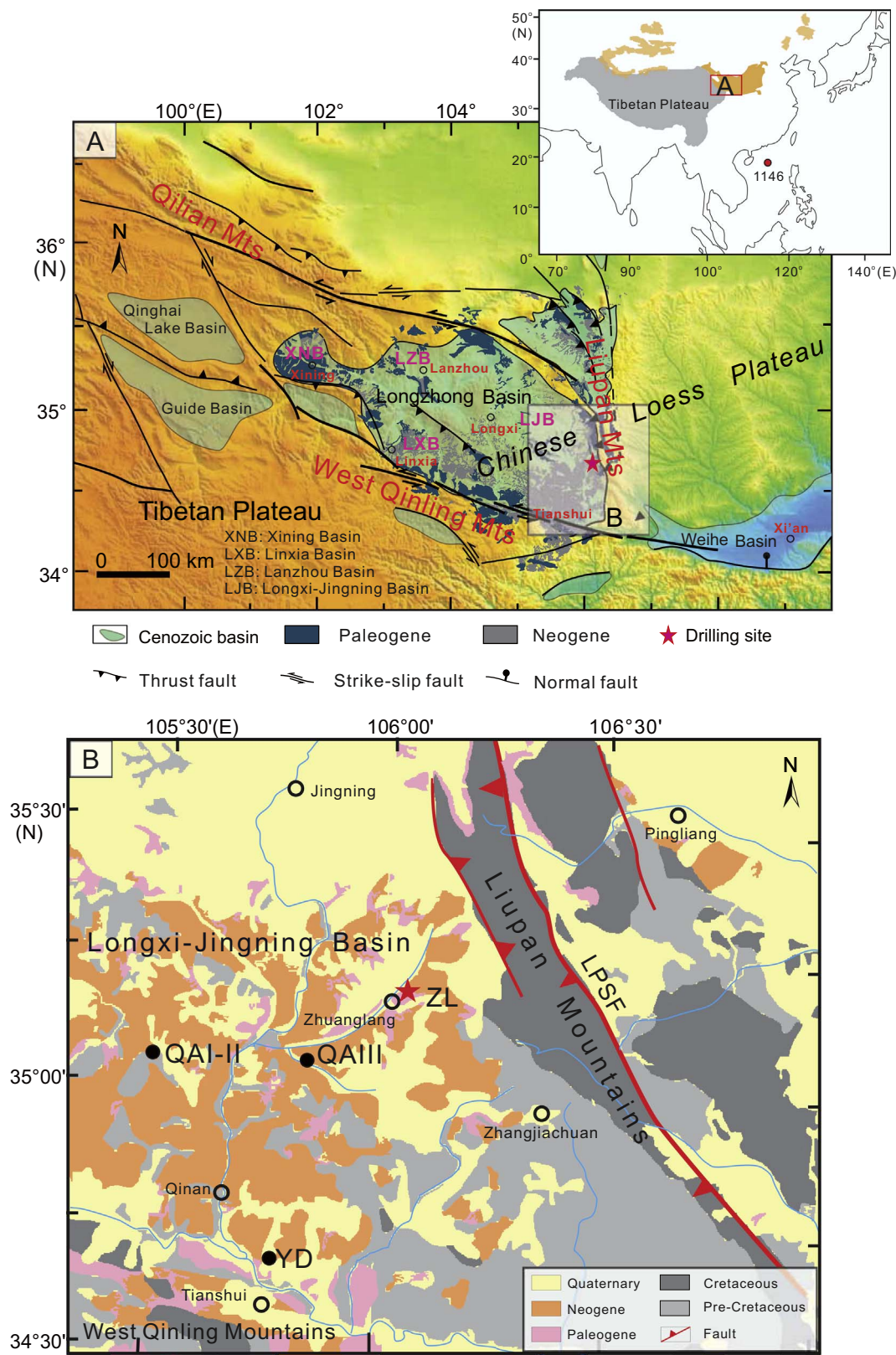


Fig. 1. Geological setting and location map of the Longzhong Basin. A) Cenozoic strata and fault distribution in the Longzhong Basin (simplified from Wang et al., 2012). Insert map shows the location of the Longzhong Basin in Asia. B) Simplified geological map of the Longxi-Jingning Sub-basin and Neogene red clay sections.

$$4 \times I(\text{illite}-10 \text{ \AA}) + I(\text{smectite}-17 \text{ \AA}) + 2 \times I(\text{kaolinite, chlorite}-7 \text{ \AA}) = 100\%. \quad (1)$$

Major element concentrations were determined using a PANalytical

PW4400 X-ray fluorescence (XRF) spectrometer after fusion of the carbonate-free fraction. About 0.6 g of the powdered clay minerals samples was fused with 6 g of dry lithium tetraborate ($\text{Li}_2\text{B}_4\text{O}_7$) at

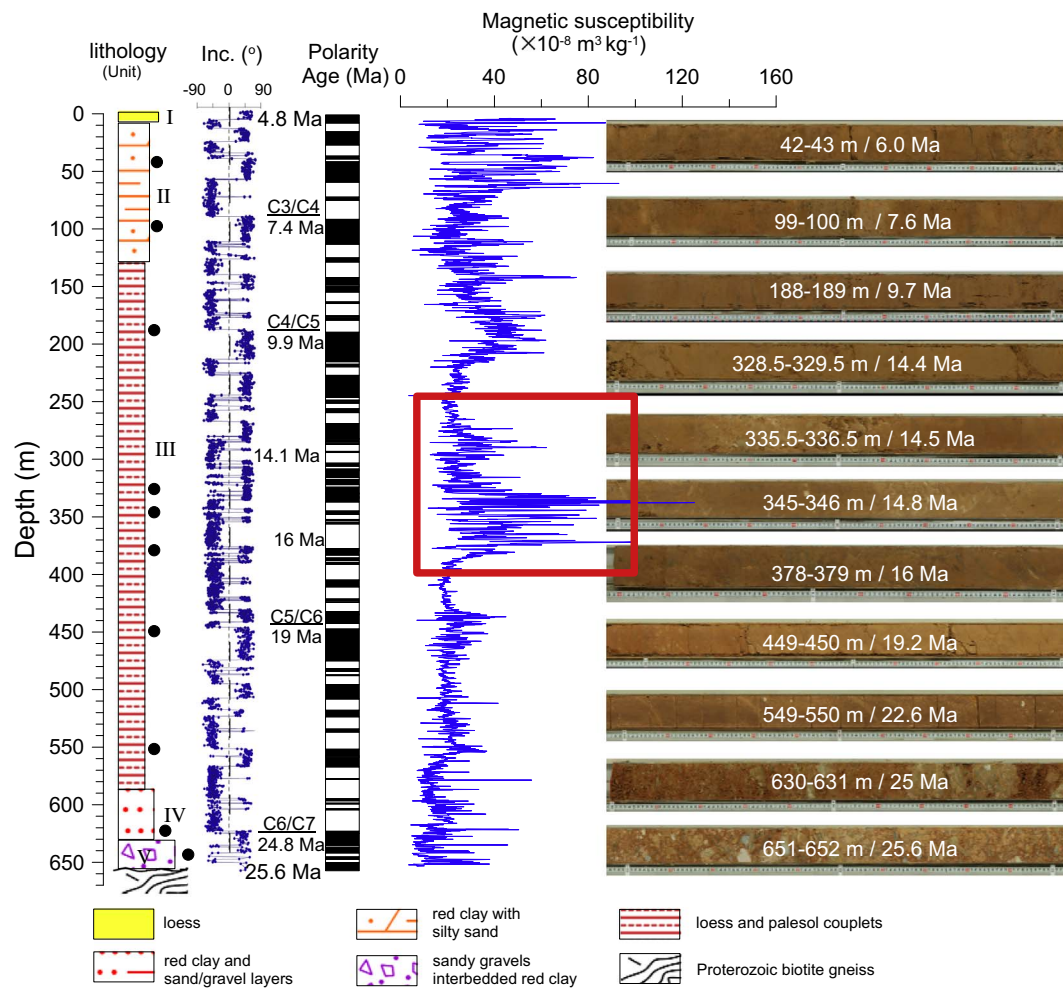


Fig. 2. Polarity, magnetic susceptibility and typical lithological image of the Zhanglang core (polarity and magnetic susceptibility from Qiang et al., 2011). The red frame indicates the study section. Solid circles show the locations of the lithological images on the right. (For interpretation of the references to color in this figure legend, the reader is referred to the web version of this article.)

950 °C. The mixed samples were placed in a Claissé Flux melting furnace and fused for 5 min at high temperature (about 1000 °C) before being formed into a glass bead. A calibration curve was established using 16 Chinese National Standard soil reference samples (GSS-1 to GSS-16) (Gu et al., 2003; Xie et al., 1985). The reproducibility of measurements was evaluated by repeated analysis of the National Standard soil reference sample GSS-8, yielding analytical uncertainties of < 3%.

The XRD and XRF analyses were carried out at the State Key Laboratory of Loess and Quaternary Geology, Institute of Earth Environment, Chinese Academy of Sciences.

4. Results

4.1. XRD analysis

The types and contents of clay minerals were mainly determined by XRD patterns with different peaks (*d*-values) and intensities (height or area of peaks) (Biscaye, 1965; Moore and Reynolds, 1997). Comparing the XRD patterns of the N and EG clays (Fig. 3), it can be seen that the majority of the 12–14.1 Å reflections from the N clay fractions shifted to 17 Å after EG. Only a small portion of the peak remained at 14.1 Å. The 17 Å and 14.1 Å diffraction peaks of the EG clays are attributed to smectite (including randomly mixed illite/smectite layers) and chlorite, respectively. Overall, the characteristic diffraction peaks appeared at 17, 14.1, 10, 7, 5, 3.57, 3.33 and 3.18 Å, respectively. Semi-

quantitative analysis indicated that the clay mineral assemblages were dominated by illite (> 60%) with minor chlorite, kaolinite and smectite (Table 1). Based on the distribution of clay minerals and their ratios (Fig. 4), the period from 17 Ma to 12 Ma can be subdivided into 3 intervals with boundaries at around 14 Ma and 16 Ma. The middle interval (16–14 Ma) is characterized by relatively high smectite and kaolinite contents, higher ratios of K/(I + Ch), and lower contents of illite, chlorite and illite 5 Å/10 Å.

4.2. XRF analysis

The geochemistry of the samples is dominated by SiO₂ (45–49%) and Al₂O₃ (20–22%) with minor MgO, K₂O (< 5%) and trace NaO (< 1%). Compared with the other intervals, we found the middle interval (16–14 Ma) to be characterized by relatively lower SiO₂, MgO, NaO, K₂O contents and K₂O/Al₂O₃ ratio, higher Al₂O₃ content and higher SiO₂/Al₂O₃ ratio (Fig. 5).

5. Discussion

5.1. Origins of the clay minerals

The origins of clay minerals can be classified as detrital or authigenic (Chamley, 1989; Fagel, 2007; Moore and Reynolds, 1997; Thiry, 2000). Detrital clay minerals are weathering products of the initial rocks on the source areas; authigenic clay minerals result from post-

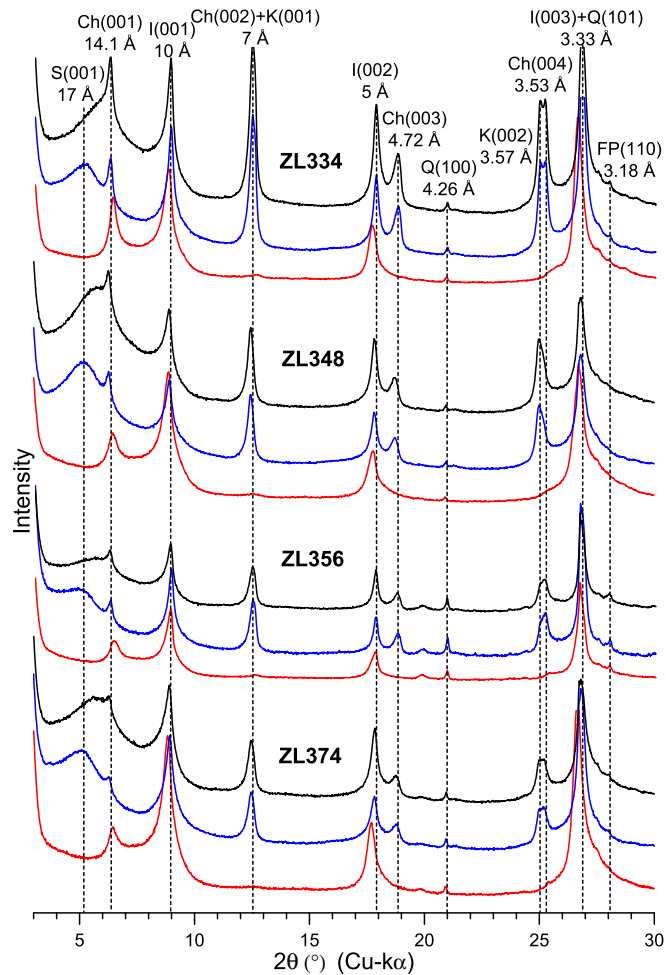


Fig. 3. XRD patterns of clay fractions from samples of the ZL red clay. Air dried (black), ethylene glycol (blue), heated (red). (For interpretation of the references to color in this figure legend, the reader is referred to the web version of this article.)

depositional diagenetic changes and hydrothermal alteration (Abdullayev and Leroy, 2016; Chamley, 1989; Gylesjö and Arnold, 2006; Hong et al., 2010; Singer, 1984; Thiry, 2000; Zeng et al., 2014). ZL drilling site is near the west pediment of the Liupan Mountains. The uplift of the Liupan Mountains, to a certain extent, could affect the sediments process. But previous thermochronological work and tectonic studies indicated that the uplift of the Liupan Mountains start from Late Miocene (10–8 Ma) (Li et al., 2013; Lin et al., 2010; Song et al., 2005, 2001; Zheng et al., 2006) or Pliocene (Zhang et al., 1991), which is younger than the period (18–14 Ma) we discuss. Therefore, the tectonic activity of the Liupan Mountains might have no effect on the sediment process. Previous sedimentological, geochemical, mineralogical and quartz morphological evidence show that the ZL red clay sequence is of eolian origin (Qiang et al., 2011). Dust materials in the ZL red clay were transported by both the northwest Asian winter monsoon and the

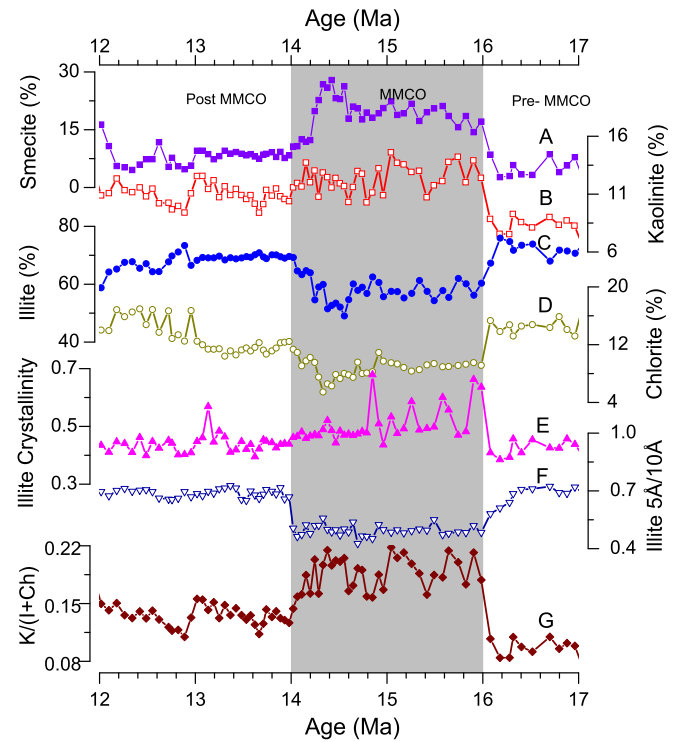


Fig. 4. Variations in clay mineral composition (%) and characteristic indices of the ZL red clay.

westerlies (Qiang et al., 2011). The diagenetic illitization of smectite requires a burial depth of > 1500 m (Chamley, 1989), a transition pressure of 900–920 kg·cm⁻², and a transition temperature of 100–140 °C (Liu, 1985). The thickness of the ZL core is only 654 m, so diagenesis will have had little or no effect due to the limited burial depth. Therefore, the clay minerals of this core are of detrital origin, which is consistent with those of the late Mio-Pliocene red clay and Quaternary loess-paleosol sediments in the Central Chinese Loess Plateau (Gylesjö and Arnold, 2006; Ji et al., 1999; Liu, 1985). Detrital clay minerals can be used to discuss variations in weathering/erosion processes related to climatic change, and then to reconstruct the paleoclimates (Chen et al., 2017; Kemp et al., 2016; Singer, 1984; Thiry, 2000).

5.2. MMCO recorded by clay minerals in the Longzhong Basin

In general, illite and chlorite are the most common clay minerals in the sediments. Illite is the weathering product of aluminosilicate minerals under weak alkaline conditions with a dry and cold climate and limited leaching. Similarly, chlorite is formed under an arid climate and alkaline conditions (Chamley, 1989; Grim, 1968). Consequently, illite and chlorite concentrations increase in cold and dry climates, and decrease during warm and humid periods (Chamley, 1989; Fagel, 2007; Grim, 1968; Gylesjö and Arnold, 2006; Liu, 1985; Zhang and Guo, 2014). In contrast, kaolinite commonly forms under warm, moist environments where intense chemical weathering can take place, while

Table 1
Clay mineral contents and characteristic indexes of the ZL red clay in the middle Miocene period.

| Period | Smectite % | Kaolinite % | Illite % | Chlorite % | Illite crystallinity °Δ2θCu Kα | Illite 5 Å/10 Å |
|----------|------------|-------------|----------|------------|-----------------------------------|--------------------|
| 17–16 Ma | 8.2 | 10.1 | 68.1 | 13.6 | 0.42 | 0.68 |
| 16–14 Ma | 12.6 | 11.4 | 63.8 | 11.8 | 0.45 | 0.54 |
| 14–12 Ma | 6.4 | 8.7 | 66.7 | 13.7 | 0.43 | 0.68 |
| Average | 9.0 | 10.0 | 66.2 | 13.1 | 0.43 | 0.63 |

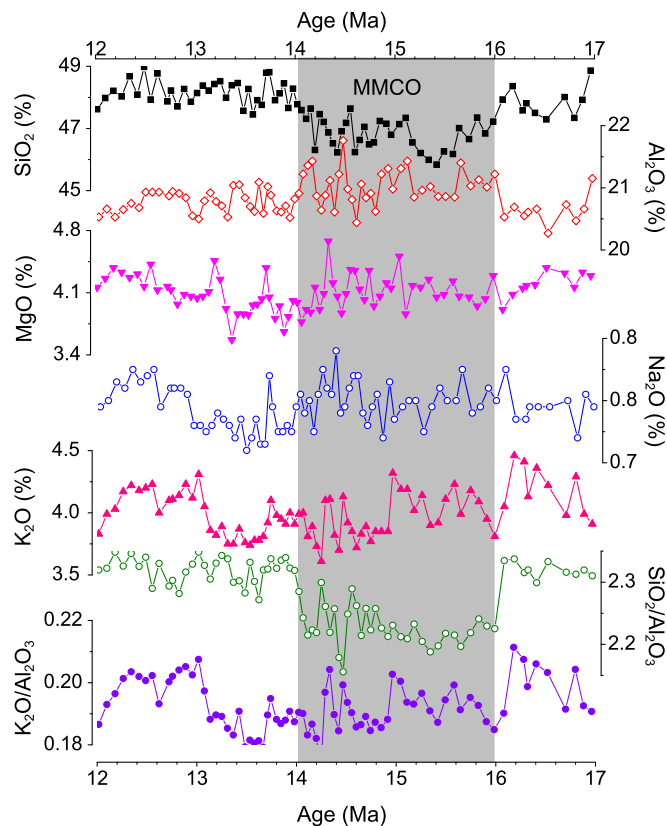


Fig. 5. Variations in elemental composition of typical clay minerals in the ZL red clay during 17–12 Ma.

smectite forms in areas with poor drainage (Chamley, 1989; Fagel, 2007; Song et al., 2014). The illite crystallinity may be determined from the full width at half-height of its (001) diffraction peak, and reflects the mineral's susceptibility to hydrolysis. To a certain extent, this indicates the moisture level (Chamley, 1989; Diemann and Wopfner, 1996; Fagel, 2007; Sheldon and Tabor, 2009). Meanwhile, the illite 5 Å/10 Å indicates the degree of weathering (Deepty and Balakrishnan, 2005; Diemann and Wopfner, 1996; Liu et al., 2014; Liu et al., 2010). The clay mineral ratio, kaolinite/(illite + chlorite), is less sensitive to the influence of external factors and is a good indicator of climatic fluctuations (Liu et al., 2010; Zeng et al., 2014; Zhang and Guo, 2014; Zhao, 2005).

In general, the dominant illite content (> 60%) of the studied section implies that the climate in this region was typically cold and dry, consistent with a global cooling trend (Zachos et al., 2001) and Asian interior aridification (Guo et al., 2002) during the Miocene. Under this global and regional cooling and arid background, the climate underwent significant fluctuations. In the middle interval, increased kaolinite and smectite contents and decreased illite and chlorite contents (Fig. 4) suggest relatively warmer and moister climatic conditions from ~16 Ma to ~14 Ma. During pedogenesis, chlorite and illite would have been converted to smectite and kaolinite under the warm and humid climate conditions, due to intense leaching and weathering. The higher illite crystallinity values (Fig. 4E), higher kaolinite/(illite + chlorite) ratio (Fig. 4G) and lower illite 5 Å/10 Å (Fig. 4F) indicate that precipitation and weathering intensity were greater during this period. At the same time, the content of SiO₂ was decreasing while that of Al₂O₃ was increasing (Fig. 5). We interpret this change as a response to the MMCO (16–14 Ma). The SiO₂/Al₂O₃ ratio (Fig. 5F) followed a declining trend during this period, showing that precipitation and weathering also gradually increased during the MMCO. The apparent dissolution characteristics or well-defined edges of the clay mineral surfaces indicated stronger chemical weathering characteristics during

the formation of the clay minerals. The warm and moist climate of the MMCO recorded by clay mineral and geochemistry is broadly consistent with magnetic susceptibility in both the ZL core (Qiang et al., 2011) and QA I-II section (Guo et al., 2002) (Fig. 1), as well as the pollen record of the YD section (Hui et al., 2011) in the Longzhong Basin. During 17.1–14.7 Ma, vegetation in the YD section was dominated by temperate to warm-temperate forests, with genera such as *Betula*, *Quercus*, and *Ulmus* again indicating a warm and humid climate (Hui et al., 2011).

Palynological analysis of a recently examined Oligocene–Pliocene stratigraphic sequence in the northern foreland basin of the Tian Shan revealed that the MMCO occurred at ca. 18–15 Ma (Sun and Zhang, 2008). However, the most prominent changes in the lithological and magnetic record of the Miocene flood-plain to channel-flood deposits from the Xining Basin, NE Tibetan Plateau occurred at 17–14 Ma (Zan et al., 2015), and high thermophilic taxa pollen percentages from the KC-1 core in the Qaidam Basin occurred at 18–14 Ma (Miao et al., 2011). The thick gypsum bed observed in the Sikouzi section in the Northern Liupan Mountains suggests a predominately dry climate during 16–15 Ma (Lin et al., 2016). Chemical Index of Alteration (CIA) values and terrigenous Mass Accumulation Rates (MARs) significantly increased at ca. 17–15 Ma in the East Monsoon region (Wan et al., 2009). Our clay mineral and geochemical record supports an MMCO at 16–14 Ma under warm and humid conditions.

5.3. Comparison with regional and global records, and possible mechanisms

Miao et al. (2012) reviewed previous literature on Cenozoic pollen and other proxies, and concluded that Miocene climatic change followed two trends in NW China. The pollen record of the KC-1 core in the Qaidam Basin (Miao et al., 2011) and Sikouzi in Ningxia (Jiang and Ding, 2008) show a cooling and drying trend, but Linxia (Ma et al., 1998), Qin'an (Guo et al., 2002) and the ZL core (Qiang et al., 2011) in the Longzhong Basin show overall trends of increasing moisture (albeit with strong fluctuations). In the ZL core, higher K/(I + Ch) (Fig. 6A) and lower chlorite (Fig. 6B) and SiO₂/Al₂O₃ (Fig. 6C) are well correlated with the higher magnetic susceptibility values in both the ZL core (Fig. 6D) (Qiang et al., 2011) and Qin'an-I section (Fig. 6E) (Guo et al., 2002) during the MMCO. The clay mineral analysis and geochemistry identified in this study support the latter trend. Our interpretation is that the warm and moist paleoenvironment was favorable to pedogenesis, generating more fine-grained magnetic minerals while also decomposing and transforming illite and chlorite, thereby yielding more smectite and kaolinite. This implies a significantly intensified summer monsoon. The pollen record from the YD section (Fig. 1B) in the south Longzhong Basin also indicated that the vegetation was dominated by trees (Fig. 6F) (Hui et al., 2011), although the warm-moist period was proposed to have occurred at a different time (from 16.5 to 15 Ma). Similar lags were also observed in marine sediments in the South China Sea, associated with intensive chemical weathering together with strong physical erosion and lower chlorite content (Fig. 6G) during the MMCO period from 17 to 15 Ma (Clift et al., 2014; Wan et al., 2009, 2007). These different lines of evidence highlight regional variability in the characteristics of the MMCO.

The paleoclimatic and paleoenvironmental characteristics of the MMCO period have been reported from other areas of China. Pollen records suggest that the lowest recorded abundances of the conifer genera *Pinus* and *Abies* and the highest abundances of *Betula*, *Juglans* and *Quercus* in the foreland basin in NW China occurred during the MMCO (Hui et al., 2011; Miao et al., 2012; Sun and Zhang, 2008). The mineralogical ratio chlorite/(chlorite + haematite + goetite) (C_{RAT}) in marine sediments of the South China Sea documents the climatic transition to wetter conditions with enhanced chemical weathering during the MMCO (Clift et al., 2014; Wan et al., 2009, 2007); at this time the erosion/deposition rate accelerated from 15.5 Ma, and the dominant clay mineral changed from smectite to illite (Clift et al., 2008;

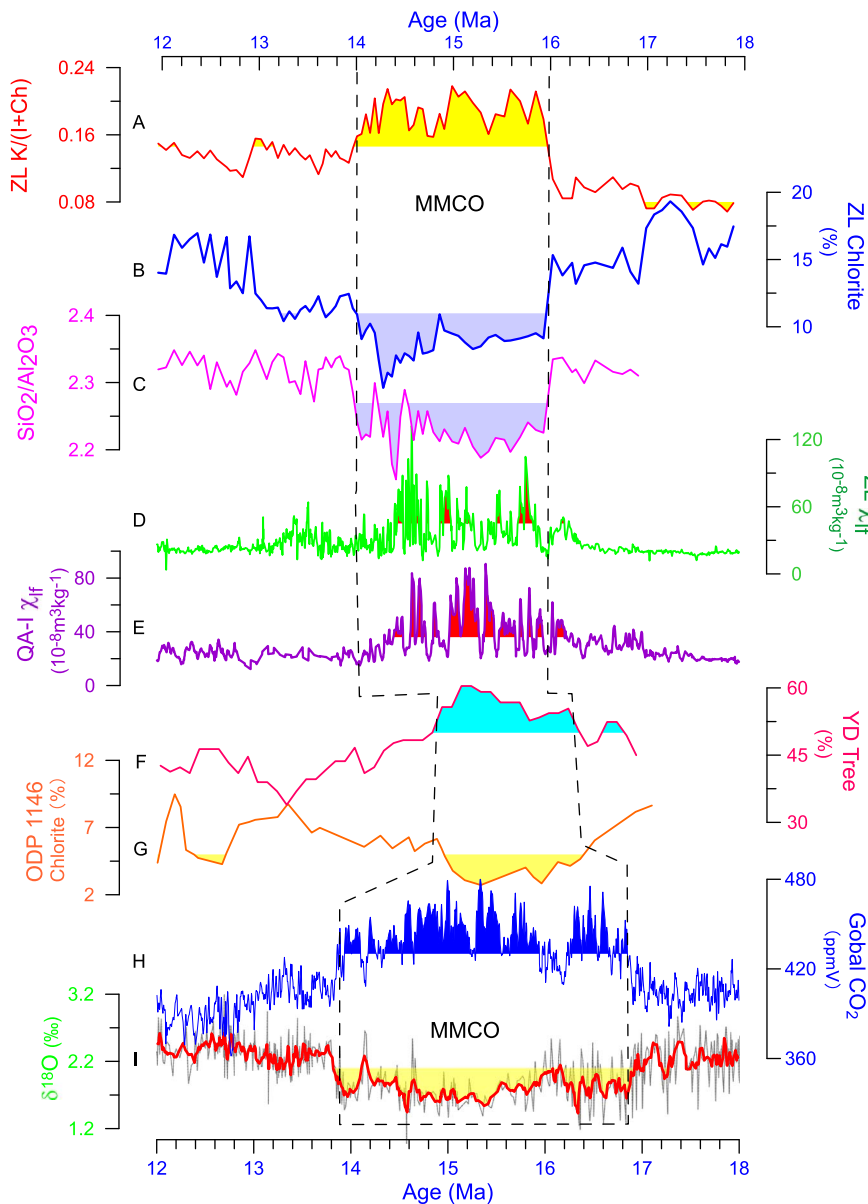


Fig. 6. Comparisons of clay minerals in the ZL red clay with regional and global climatic records during the MMCO.

Clift and Plumb, 2008; Clift et al., 2014). The lower chlorite contents both in the ZL core (Fig. 6C) and at ODP Site 1146 (Fig. 6G) (location see Fig. 1A inserted map) (Wan et al., 2007) during the MMCO indicate that physical and chemical weathering were relatively strong and the climate was humid.

Previous paleoclimate studies have identified higher temperature and precipitation, lush vegetation and higher productivity during the MMCO in Europe (Böhme, 2003; Harzhauser et al., 2011; Larsson et al., 2011). The pollen and fossil records reveal that the proportion of pyrophilous and hygrophilous species increased, while arctophilous species decreased in America and Antarctica; glacial retreat and glaciated landforms were widely distributed in the polar regions (Escutia et al., 2005; Kaandorp et al., 2005; Lewis et al., 2007, 2008). By comparing > 40 ODP drilling holes, it was found that the deep-sea $\delta^{18}\text{O}$ values (Fig. 6I) decreased significantly, $\delta^{13}\text{C}$ values increased and the CO_2 concentration reached a peak (Fig. 6H); the Antarctic ice sheet retreated strongly; and global sea level rose during the MMCO. The warm and humid paleoclimate is the main characteristic of the MMCO (Zachos et al., 2008; Zachos et al., 2001). The sediment records reveal that global average temperature during the MMCO stage reached 18.4°C with an ocean temperature about 6°C higher than present at

high latitudes (Flower and Kennett, 1994; You et al., 2009). Therefore, our ZL red clay section provides new clay mineral evidence for the global MMCO.

Global cooling and uplift of the Tibetan Plateau were the main factors driving the evolution of the MMCO (both temperature and moisture) in NW China (Miao et al., 2011, 2012; Sun et al., 2015; Zhang et al., 2015). However, previously published thermochronological data from NW China (mainly the northeastern Tibetan Plateau and its adjacent areas) suggest that two phases of rapid uplift of northern Tibetan Plateau occurred at around 24–17 Ma (Jolivet et al., 2001; Lu et al., 2012) and 13–7 Ma (Lease et al., 2011; Sun et al., 2015; Zhang et al., 2017; Zheng et al., 2006). Therefore, the uplift of northern Tibetan Plateau might have no or limited influence on the MMCO event, and instead global climatic fluctuation might have played the key role in its occurrence.

Global cooling and expansion of the Antarctic Ice-sheets began prior to the Miocene and continued until the middle Miocene, ending with a period of global warming between 17 Ma and 14 Ma ago (Zachos et al., 2001). Subsequently, the East Antarctic ice sheet underwent a major expansion caused renewed global cooling. Global warming was a key factor causing the MMCO (Böhme, 2003; Clift et al., 2014; Lewis et al.,

2007; Miao et al., 2012). Under this global warming, the zonal gradient of temperature decreased and there was greater transfer of moisture and heat from low latitudes to high latitudes, leading to increased precipitation at high latitudes; at the same time, global warming melted a large proportion of the Antarctic Ice Sheet, causing sea level rise and greater inland transport of moisture and heat. Increasing CO₂ concentration (Fig. 6H) is regarded as another important factor in the formation of the MMCO (Beerling et al., 2009; Tripathi et al., 2011; You et al., 2009). The results of numerical simulations show that a CO₂ concentration of 460–580 ppm could have been responsible for the MMCO, which is consistent with the relatively high value of CO₂ concentration reported during that period (Fig. 6H) (Beerling et al., 2009; Van de Wal et al., 2011; You et al., 2009). Overall, the MMCO was a global warming event under the global cooling background during the Cenozoic period, and caused enhanced chemical weathering in global terrestrial sediments and high productivity in marine sediments.

6. Conclusions

X-ray diffraction analysis shows that clay minerals in the ZL core are dominated by illite, with minor smectite, chlorite and kaolinite. The clay mineral assemblages reveal that the MMCO occurred at 16–14 Ma, characterized by relatively higher contents of kaolinite and smectite, higher illite crystallinity and kaolinite/(illite + chlorite) ratio, and lower chlorite and illite contents, which indicate a warm and moist climatic environment during this period. When compared with the local and global records, we find that clay mineral records reflect regional climatic variability superimposed on global climatic change during the MMCO. We infer that the warm-moist climate characteristics are the result of high CO₂ concentration and global warming, rather than the effects of the uplift of the Tibetan Plateau.

Acknowledgments

We gratefully acknowledge the Editor-in-Chief Thomas Algeo and guest editor Hanlie Hong and two anonymous reviewers for constructive comments and suggestions, and also thank Dr. Dave Chandler for language editing and polishing. This work was supported by the National Natural Science Foundation of China (Nos. 41290253, 41572162), Shandong Provincial Natural Science Foundation (No. ZR2017BD017), Xi'an Centre of Geological Survey, China Geological Survey (CGS Diaosheng [2017]0438) and International Partnership Program of Chinese Academy of Sciences [No: 132B61KYS20160002].

References

- Abdullayev, E., Leroy, S.A.G., 2016. Provenance of clay minerals in the sediments from the Pliocene Productive Series, western South Caspian Basin. *Mar. Pet. Geol.* 73, 517–527.
- Alonso-Zarza, A.M., Zhao, Z., Song, C.H., Li, J.J., Zhang, J., Martín-Pérez, A., Martín-García, R., Wang, X.X., Zhang, Y., Zhang, M.H., 2009. Mudflat/distal fan and shallow lake sedimentation (upper Vallesian-Turolian) in the Tianshui Basin, Central China: evidence against the late Miocene eolian loess. *Sediment. Geol.* 222, 42–51.
- Ao, H., Zhang, P., Dekkers, M.J., Roberts, A.P., An, Z., Li, Y., Lu, F., Lin, S., Li, X., 2016. New magnetochronology of Late Miocene mammal fauna, NE Tibetan Plateau, China: mammal migration and paleoenvironments. *Earth Planet. Sci. Lett.* 434, 220–230.
- Beerling, D.J., Fox, A., Anderson, C.W., 2009. Quantitative uncertainty analyses of ancient atmospheric CO₂ estimates from fossil leaves. *Am. J. Sci.* 309, 775–787.
- Biscaye, P.E., 1965. Mineralogy and sedimentation of recent deep-sea clay in the Atlantic Ocean and adjacent seas and oceans. *Geol. Soc. Am. Bull.* 76, 803–832.
- Böhme, M., 2003. The Miocene Climatic Optimum: evidence from ectothermic vertebrates of Central Europe. *Palaeogeogr. Palaeoclimatol. Palaeoecol.* 195, 389–401.
- Chamley, H., 1989. *Clay Sedimentology*. Springer-Verlag, Heidelberg.
- Chen, Q., Liu, Z., Kissel, C., 2017. Clay mineralogical and geochemical proxies of the East Asian summer monsoon evolution in the South China Sea during Late Quaternary. *Sci. Rep.* 7, e42083.
- Clift, P.D., Plumb, R.A., 2008. *The Asian Monsoon: Causes, History and Effects*. Cambridge University Press, Cambridge.
- Clift, P.D., Hodges, K.V., Heslop, D., Hannigan, R., Van Long, H., Calves, G., 2008. Correlation of Himalayan exhumation rates and Asian monsoon intensity. *Nat. Geosci.* 1, 875–880.
- Clift, P.D., Wan, S., Blusztajn, J., 2014. Reconstructing chemical weathering, physical erosion and monsoon intensity since 25 Ma in the northern South China Sea: a review of competing proxies. *Earth-Sci. Rev.* 130, 86–102.
- Deepthi, R., Balakrishnan, S., 2005. Climatic control on clay mineral formation: evidence from weathering profiles developed on either side of the Western Ghats. *J. Earth Syst. Sci.* 114, 545–556.
- Diemann, B., Wopfner, H., 1996. Petrographic and diagenetic signatures of climatic change in peri- and postglacial Karoo Sediments of SW Tanzania. *Palaeogeogr. Palaeoclimatol. Palaeoecol.* 125, 5–25.
- Dupont-Nivet, G., Krijgsman, W., Langereis, C.G., Abels, H.A., Dai, S., Fang, X., 2007. Tibetan plateau aridification linked to global cooling at the Eocene-Oligocene transition. *Nature* 445, 635–638.
- Escutia, C., De Santis, L., Donda, F., Dunbar, R.B., Cooper, A.K., Brancolini, G., Eitrem, S.L., 2005. Cenozoic ice sheet history from East Antarctic Wilkes Land continental margin sediments. *Glob. Planet. Chang.* 45, 51–81.
- Fagel, N., 2007. Clay minerals, deep circulation and climate. *Proxies in Late Cenozoic. Paleoclimatology* 1, 139–184.
- Fang, X.M., Garzione, C., Van der Voo, R., Li, J.J., Fan, M.J., 2003. Flexural subsidence by 29 Ma on the NE edge of Tibet from the magnetostratigraphy of Linxia Basin, China. *Earth Planet. Sci. Lett.* 210, 545–560.
- Flower, B.P., Kennett, J.P., 1994. The middle Miocene climatic transition - East Antarctic ice-sheet development, deep-ocean circulation and global carbon cycling. *Palaeogeogr. Palaeoclimatol. Palaeoecol.* 108, 537–555.
- Gao, Y., Wang, C., Liu, Z., Zhao, B., Zhang, X., 2013. Clay mineralogy of the middle Mingshui Formation (upper Campanian to lower Maastrichtian) from the SKIn borehole in the Songliao Basin, NE China: implications for palaeoclimate and provenance. *Palaeogeogr. Palaeoclimatol. Palaeoecol.* 385, 162–170.
- George, A.D., Marshall, S.J., Wyrwoll, K.-H., Jie, C., Yanchou, L., 2001. Miocene cooling in the northern Qilian Shan, northeastern margin of the Tibetan Plateau, revealed by apatite fission-track and vitrinite-reflectance analysis. *Geology* 29, 939–942.
- Goldner, A., Herold, N., Huber, M., 2014. The challenge of simulating the warmth of the mid-Miocene climatic optimum in CESM1. *Clim. Past* 10, 523–536.
- Grim, R.E., 1968. *Clay Mineralogy*. McGraw-Hill, New York.
- Gu, T., Bu, W., Yan, W., Shi, C., Yan, M., 2003. New series of soil geochemical reference materials (GSS 10-16) from the main overburden region in China. *Geostand. Newslett.* 27, 197–202.
- Guo, Z.T., Ruddiman, W.F., Hao, Q.Z., Wu, H.B., Qiao, Y.S., Zhu, R.X., Peng, S.Z., Wei, J.J., Yuan, B.Y., Liu, T.S., 2002. Onset of Asian desertification by 22 Myr ago inferred from loess deposits in China. *Nature* 416, 159–163.
- Guo, Z.T., Ge, J.Y., Xiao, G.Q., Hao, Q.Z., Wu, H.B., Zhan, T., Liu, L., Qin, L., Zeng, F.M., Yuan, B.Y., 2010. Comment on “Mudflat/distal fan and shallow lake sedimentation (upper Vallesian-Turolian) in the Tianshui Basin, Central China: evidence against the late Miocene eolian loess” by A.M. Alonso-Zarza, Z. Zhao, C.H. Song, J.J. Li, J. Zhang, A. Martín-Pérez, R. Martín-García, X.X. Wang, Y. Zhang and M.H. Zhang [Sedimentary Geology 222 (2009) 42–51]. *Sediment. Geol.* 230, 86–89.
- Gylesjö, S., Arnold, E., 2006. Clay mineralogy of a red clay-loess sequence from Lingtai, the Chinese Loess Plateau. *Glob. Planet. Chang.* 51, 181–194.
- Hao, Q., Guo, Z., 2007. Magnetostratigraphy of an early-middle Miocene loess-soil sequence in the western Loess Plateau of China. *Geophys. Res. Lett.* 34, L18305. <http://dx.doi.org/10.1029/2007GL031162>.
- Harzhauser, M., Piller, W.E., Müllegger, S., Grunert, P., Micheels, A., 2011. Changing seasonality patterns in Central Europe from Miocene Climate Optimum to Miocene Climate Transition deduced from the Crassostrea isotope archive. *Glob. Planet. Chang.* 76, 77–84.
- Holbourn, A., Kuhnt, W., Lyle, M., Schneider, L., Romero, O., Andersen, N., 2013. Middle Miocene climate cooling linked to intensification of eastern equatorial Pacific upwelling. *Geology* 42, 19–22.
- Hong, H.L., Zhang, K.X., Li, Z.H., 2010. Climatic and tectonic uplift evolution since similar to 7 Ma in Gyirong basin, southwestern Tibet plateau: clay mineral evidence. *Int. J. Earth Sci.* 99, 1305–1315.
- Hong, H., Fang, Q., Wang, C., Churchman, G.J., Zhao, L., Gong, N., Yin, K., 2017. Clay mineralogy of altered tephra beds and facies correlation between the Permian-Triassic boundary stratigraphic sets, Guizhou, south China. *Appl. Clay Sci.* 143, 10–21.
- Hui, Z.C., Li, J.J., Xu, Q.H., Song, C.H., Zhang, J., Wu, F., Zhao, Z., 2011. Miocene vegetation and climatic changes reconstructed from a sporopollen record of the Tianshui Basin, NE Tibetan Plateau. *Palaeogeogr. Palaeoclimatol. Palaeoecol.* 308, 373–382.
- Ji, J., Chen, J., Lu, H., 1999. Origin of illite in the loess from the Luochuan area, Loess Plateau, central China. *Clay Miner.* 34, 525–532.
- Jiang, H., Ding, Z., 2008. A 20 Ma pollen record of East-Asian summer monsoon evolution from Guyuan, Ningxia, China. *Palaeogeogr. Palaeoclimatol. Palaeoecol.* 265, 30–38.
- Jolivet, M., Brunel, M., Seward, D., Xu, Z., Yang, J., Roger, F., Tapponnier, P., Malavieille, J., Arnaud, N., Wu, C., 2001. Mesozoic and Cenozoic tectonics of the northern edge of the Tibetan plateau: fission-track constraints. *Tectonophysics* 343, 111–134.
- Kaandorp, R.J.G., Vonhof, H.B., Wesselingh, F.P., Pittman, L.R., Kroon, D., van Hinte, J.E., 2005. Seasonal Amazonian rainfall variation in the Miocene Climate Optimum. *Palaeogeogr. Palaeoclimatol. Palaeoecol.* 221, 1–6.
- Kemp, S.J., Ellis, M.A., Mountney, I., Kender, S., 2016. Palaeoclimatic implications of high-resolution clay mineral assemblages preceding and across the onset of the Palaeocene-Eocene Thermal Maximum, North Sea Basin. *Clay Miner.* 51, 793–813.
- Larsson, L.M., Dybkjær, K., Rasmussen, E.S., Piasecki, S., Utescher, T., Vajda, V., 2011. Miocene climate evolution of northern Europe: a palynological investigation from Denmark. *Palaeogeogr. Palaeoclimatol. Palaeoecol.* 309, 161–175.
- Lease, R.O., Burbank, D.W., Clark, M.K., Farley, K.A., Zheng, D., Zhang, H., 2011. Middle

- Miocene reorganization of deformation along the northeastern Tibetan Plateau. *Geology* 39, 359–362.
- Lewis, A.R., Marchant, D.R., Ashworth, A.C., Hemming, S.R., Machlus, M.L., 2007. Major middle Miocene global climate change: evidence from East Antarctica and the Transantarctic Mountains. *Geol. Soc. Am. Bull.* 119, 1449–1461.
- Lewis, A.R., Marchant, D.R., Ashworth, A.C., Hedenas, L., Hemming, S.R., Johnson, J.V., Leng, M.J., Machlus, M.L., Newton, A.E., Raine, J.L., Willenbring, J.K., Williams, M., Wolfe, A.P., 2008. Mid-Miocene cooling and the extinction of tundra in continental Antarctica. *Proc. Natl. Acad. Sci. U. S. A.* 105, 10676–10680.
- Li, J., Zhang, J., Song, C., Zhao, Z., Zhang, Y., Wang, X., Zhang, J., Cui, Q., 2006. Miocene Bahean stratigraphy in the Longzhong Basin, northern central China and its implications in environmental change. *Sci. China Ser. D* 49, 1270–1279.
- Li, Y., Song, Y., Qian, L., Li, X., Qiang, X., An, Z., 2013. Paleomagnetic and fission-track dating of a Late Cenozoic red earth section in the Liupan Shan and associated tectonic implications. *J. Earth Sci.* 24, 506–518.
- Liang, M., Wang, Z., Zhou, S., Zong, K., Hu, Z., 2014. The provenance of Gansu Group in Longxi region and implications for tectonics and paleoclimate. *Sci. China Earth Sci.* 57, 1221–1228.
- Lin, X., Chen, H., Wyrwoll, K.-H., Cheng, X., 2010. Commencing uplift of the Liupan Shan since 9.5 Ma: evidences from the Sikouzi section at its east side. *J. Asian Earth Sci.* 37, 350–360.
- Lin, X.B., Wyrwoll, K.H., Chen, H.L., Cheng, X.G., 2016. On the timing and forcing mechanism of a mid-Miocene arid climate transition at the NE margins of the Tibetan Plateau: stratigraphic and sedimentologic evidence from the Sikouzi Section. *Int. J. Earth Sci.* 105, 1039–1049.
- Liu, T.S., 1985. *Loess and the Environment*. Science Press, Beijing.
- Liu, Z.F., Trentesaux, A., Clemens, S.C., Colin, C., Wang, P., Huang, B., Boulay, S., 2003. Clay mineral assemblages in the northern South China Sea: implications for East Asian monsoon evolution over the past 2 million years. *Mar. Geol.* 201, 133–146.
- Liu, Z.F., Colin, C., Trentesaux, A., Blamart, D., Bassinot, F., Siani, G., Sicre, M.-A., 2004. Erosional history of the eastern Tibetan Plateau since 190 kyr ago: clay mineralogical and geochemical investigations from the southwestern South China Sea. *Mar. Geol.* 209, 1–18.
- Liu, Z.F., Colin, C., Li, X.J., Zhao, Y.L., Tuo, S., Chen, Z., Siringan, F.P., Liu, J.T., Huang, C.-Y., You, C.-F., Huang, K.-F., 2010. Clay mineral distribution in surface sediments of the northeastern South China Sea and surrounding fluvial drainage basins: source and transport. *Mar. Geol.* 277, 48–60.
- Liu, S.F., Shi, X.F., Fang, X.S., Dou, Y.G., Liu, Y.G., Wang, X.C., 2014. Spatial and temporal distributions of clay minerals in mud deposits on the inner shelf of the East China Sea: implications for paleoenvironmental changes in the Holocene. *Quat. Int.* 349, 270–279.
- Liu, S.P., Li, J.J., Stockli, D.F., Seng, C.H., Nie, J.S., Peng, T.J., Wang, X.X., He, K., Hui, Z.C., Zhang, J., 2015. Late Tertiary reorganizations of deformation in northeastern Tibet constrained by stratigraphy and provenance data from eastern Longzhong Basin. *J. Geophys. Res. Solid Earth* 120, 5804–5821.
- Lu, H.J., Wang, E., Shi, X.H., Meng, K., 2012. Cenozoic tectonic evolution of the Elashan range and its surroundings, northern Tibetan Plateau as constrained by paleomagnetism and apatite fission track analyses. *Tectonophysics* 580, 150–161.
- Ma, Y.Z., Li, J.J., Fan, X.M., 1998. Pollen-based vegetational and climatic records during 30.6 to 5.0 My from Linxia area, Gansu (in Chinese). *Chin. Sci. Bull.* 43, 301–304.
- Miao, Y.F., Fang, X.M., Herrmann, M., Wu, F.L., Zhang, Y.Z., Liu, D.L., 2011. Miocene pollen record of KC-1 core in the Qaidam Basin, NE Tibetan Plateau and implications for evolution of the East Asian monsoon. *Palaeogeogr. Palaeoclimatol. Palaeoecol.* 299, 30–38.
- Miao, Y.F., Herrmann, M., Wu, F.L., Yan, X.L., Yang, S.L., 2012. What controlled Mid–Late Miocene long-term aridification in Central Asia? — global cooling or Tibetan Plateau uplift: a review. *Earth-Sci. Rev.* 112, 155–172.
- Miller, K.G., Wright, J.D., Fairbanks, R.G., 1991. Unlocking the Ice House: Oligocene–Miocene oxygen isotopes, eustasy, and margin erosion. *J. Geophys. Res. Solid Earth* 96, 6829–6848.
- Moore, D.M., Reynolds, R.C., 1997. *X-ray Diffraction and the Identification and Analysis of Clay Minerals*, second edition. Oxford University Press, New York.
- NEA, 2010. *Analysis Method for Clay Minerals and Ordinary Non-clay Minerals in Sedimentary Rocks by the X-ray Diffraction*. Chinese Oil Gas Industry Standard, SY/T 5163–2010. National Energy Administration, Beijing, pp. 1–12.
- Pal, D.K., Bhattacharyya, T., Sinha, R., Srivastava, P., Dasgupta, A.S., Chandran, P., Ray, S.K., Nimje, A., 2012. Clay minerals record from Late Quaternary drill cores of the Ganga Plains and their implications for provenance and climate change in the Himalayan foreland. *Palaeogeogr. Palaeoclimatol. Palaeoecol.* 356–357, 27–37.
- Petschick, R., 2000. *MacDiff 4.2.5*. Available at: <http://servermac.geologie.uni-frankfurt.de/Staff/Hompages/Petschick/classicsoftware.html>.
- Pierce, E.L., van de Flierdt, T., Williams, T., Hemming, S.R., Cook, C.P., Passchier, S., 2017. Evidence for a dynamic East Antarctic ice sheet during the mid-Miocene climate transition. *Earth Planet. Sci. Lett.* 478, 1–13.
- Qiang, X.K., An, Z.S., Song, Y.G., Chang, H., Sun, Y.B., Liu, W.G., Ao, H., Dong, J.B., Fu, C.F., Wu, F., Lu, F.Y., Cai, Y.J., Zhou, W.J., Cao, J.J., Xu, X.W., Ai, L., 2011. New eolian red clay sequence on the western Chinese Loess Plateau linked to onset of Asian desertification about 25 Ma ago. *Sci. China Earth Sci.* 54, 136–144.
- Qu, Y., Cai, T., 1984. The Tertiary System of Gansu Province. *Gansu Geol.* 1–40.
- Sheldon, N.D., Tabor, N.J., 2009. Quantitative paleoenvironmental and paleoclimatic reconstruction using paleosols. *Earth-Sci. Rev.* 95, 1–52.
- Singer, A., 1984. The paleoclimatic interpretation of clay minerals in sediments—a review. *Earth-Sci. Rev.* 21, 251–293.
- Song, Y.G., Fang, X.M., Li, J.J., An, Z.S., Miao, X.D., 2001. The Late Cenozoic uplift of the Liupan Shan, China. *Sci. China Ser. D Earth Sci.* 44, 176–184.
- Song, Y.G., Fang, X.M., Dong, H.M., Qiang, X.K., Chang, H., Fu, C.F., Fu, K.D., 2005. Geochronological and stratigraphical evidences for the uplift of the Liupan Shan, Northeastern boundary of the Tibetan Plateau. In: *IEEE International Geoscience and Remote Sensing Symposium*. Institute of Electrical and Electronics Engineers Inc., Seoul, Korea, pp. 5223–5226.
- Song, E.P., Zhang, K.X., Chen, J.J., Wang, C.W., Jiang, G.L., Yin, K., Hong, H.L., Churchman, J.G., 2014. Clay mineralogy and its paleoclimatic significance of the Oligocene–Miocene Sediments in the Gerze Basin, Tibet. *Acta. Geol. Sin.-Engl.* 88, 1579–1591.
- Sun, J.M., Zhang, Z.Q., 2008. Palynological evidence for the Mid-Miocene Climatic Optimum recorded in Cenozoic sediments of the Tian Shan Range, northwestern China. *Glob. Planet. Chang.* 64, 53–68.
- Sun, Y., Ma, L., Bloemendal, J., Clemens, S., Qiang, X., An, Z., 2015. Miocene climate change on the Chinese Loess Plateau: possible links to the growth of the northern Tibetan Plateau and global cooling. *Geochim. Geophys. Geosyst.* 16, 2097–2108.
- Thiry, M., 2000. Palaeoclimatic interpretation of clay minerals in marine deposits—an outlook from the continental origin. *Earth-Sci. Rev.* 49, 201–221.
- Tripathi, A.K., Roberts, C.D., Eagle, R.A., Li, G., 2011. A 20 million year record of planktic foraminiferal B/Ca ratios: systematics and uncertainties in pCO₂ reconstructions. *Geochim. Cosmochim. Acta* 75, 2582–2610.
- Turco, E., Hilgen, F.J., Lourens, L.J., Shackleton, N.J., Zachariasse, W.J., 2001. Punctuated evolution of global climate cooling during the Late Middle to Early Late Miocene: high-resolution planktonic foraminiferal and oxygen isotope records from the Mediterranean. *Paleoceanography* 16, 405–423.
- Van de Wal, R.S.W., De Boer, B., Lourens, L.J., Köhler, P., Bintanja, R., 2011. Reconstruction of a continuous high-resolution CO₂ record over the past 20 million years. *Clim. Past* 7, 1459–1469.
- Wan, S.M., Li, A.C., Clift, P.D., Stuetz, J.-B.W., 2007. Development of the East Asian monsoon: mineralogical and sedimentological records in the northern South China Sea since 20 Ma. *Palaeogeogr. Palaeoclimatol. Palaeoecol.* 254, 561–582.
- Wan, S., Kürschner, W.M., Clift, P.D., Li, A., Li, T., 2009. Extreme weathering/erosion during the Miocene Climatic Optimum: evidence from sediment record in the South China Sea. *Geophys. Res. Lett.* 36, L19706. <http://dx.doi.org/10.1029/2009GL040279>.
- Wang, C., Hong, H.L., Song, B.W., Yin, K., Li, Z.H., Zhang, K.X., Ji, J.L., 2011. The early-Eocene climate optimum (EECO) event in the Qaidam basin, northwest China: clay evidence. *Clay Miner.* 46, 649–661.
- Wang, X., Zattin, M., Li, J., Song, C., Peng, T., Liu, S., Liu, B., 2011. Eocene to Pliocene exhumation history of the Tianshui-Huicheng region determined by Apatite fission track thermochronology: implications for evolution of the northeastern Tibetan Plateau margin. *J. Asian Earth Sci.* 42, 97–110.
- Wang, W., Kirby, E., Peizhen, Z., Dewen, Z., Guangliang, Z., Huiping, Z., Wenjun, Z., Chizhang, C., 2012. Tertiary basin evolution along the northeastern margin of the Tibetan Plateau: evidence for basin formation during Oligocene transtension. *Geol. Soc. Am. Bull.* 125, 377–400.
- Wang, C., Hong, H., Li, Z., Yin, K., Xie, J., Liang, G., Song, B., Song, E.P., Zhang, K., 2013. The Eocene–Oligocene climate transition in the Tarim Basin, Northwest China: evidence from clay mineralogy. *Appl. Clay Sci.* 74, 10–19.
- Wang, W., Zhang, P., Liu, C., Zheng, D., Yu, J., Zheng, W., Wang, Y., Zhang, H., Chen, X., 2016. Pulsed growth of the West Qinling at ~30 Ma in northeastern Tibet: evidence from Lanzhou Basin magnetostratigraphy and provenance. *J. Geophys. Res. Solid Earth* 121, 7754–7774.
- Wang, Z., Liang, M., Sun, Y., Dai, G., 2016. Cenozoic tectonic and geomorphic evolution of the Longxi region in northeastern Tibetan Plateau interpreted from detrital zircon. *Sci. China Earth Sci.* 60, 256–267.
- Xiao, G., Guo, Z., Dupont-Nivet, G., Lu, H., Wu, N., Ge, J., Hao, Q., Peng, S., Li, F., Abels, H.A., Zhang, K., 2012. Evidence for northeastern Tibetan Plateau uplift between 25 and 20 Ma in the sedimentary archive of the Xining Basin, Northwestern China. *Earth Planet. Sci. Lett.* 317–318, 185–195.
- Xie, X., Yan, M., Li, L., Shen, H., 1985. Usable values for Chinese standard reference samples of stream sediments, soils, and rocks: GSD 9-12, GSS 1-8 and GSR 1-6. *Geostand. Newslett.* 9, 277–280.
- Xu, G.Z., Deconinck, J.F., Feng, Q.L., Baudin, F., Pellenard, P., Shen, J., Bruneau, L., 2017. Clay mineralogical characteristics at the Permian–Triassic Shangsi section and their paleoenvironmental and/or paleoclimatic significance. *Palaeogeogr. Palaeoclimatol. Palaeoecol.* 474, 152–163.
- You, Y., Huber, M., Müller, R.D., Poulsen, C.J., Ribbe, J., 2009. Simulation of the middle miocene climate optimum. *Geophys. Res. Lett.* 36, L04702. <http://dx.doi.org/10.1029/2008GL036571>.
- Zachos, J.C., Pagani, M., Sloan, L., Thomas, E., Billups, K., 2001. Trends, rhythms, and aberrations in global climate 65 Ma to present. *Science* 292, 686–693.
- Zachos, J.C., Dickens, G.R., Zeebe, R.E., 2008. An early Cenozoic perspective on greenhouse warming and carbon-cycle dynamics. *Nature* 451, 279–283.
- Zan, J.B., Fang, X.M., Yan, M.D., Zhang, W.L., Lu, Y., 2015. Lithologic and rock magnetic evidence for the Mid-Miocene Climatic Optimum recorded in the sedimentary archive of the Xining Basin, NE Tibetan Plateau. *Palaeogeogr. Palaeoclimatol. Palaeoecol.* 431, 6–14.
- Zeng, M.X., Song, Y.G., An, Z.S., Chang, H., Li, Y., 2014. Clay mineral records of the Erlangjian drill core sediments from the Lake Qinghai Basin, China. *Sci. China Earth Sci.* 57, 1846–1859.
- Zhan, T., Guo, Z., Wu, H., Ge, J., Zhou, X., Wu, C., Zeng, F., 2010. Thick Miocene eolian deposits on the Huajialing Mountains: the geomorphic evolution of the western Loess Plateau. *Sci. China Earth Sci.* 54, 241–248.
- Zhang, C.X., Guo, Z.T., 2014. Clay mineral changes across the Eocene–Oligocene transition in the sedimentary sequence at Xining occurred prior to global cooling. *Palaeogeogr. Palaeoclimatol. Palaeoecol.* 411, 18–29.
- Zhang, P., Burchfiel, B.C., Molnar, P., Zhang, W., Jiao, D., Deng, Q., Wang, Y., Royden, L.,

- Song, F., 1991. Amount and style of Late Cenozoic Deformation in the Liupan Shan Area, Ningxia Autonomous Region, China. *Tectonics* 10, 1111–1129.
- Zhang, Y.B., Sun, D.H., Li, Z.J., Wang, F., Wang, X., Li, B.F., Guo, F., Wu, S., 2014. Cenozoic record of aeolian sediment accumulation and aridification from Lanzhou, China, driven by Tibetan Plateau uplift and global climate. *Glob. Planet. Chang.* 120, 1–15.
- Zhang, C.X., Xiao, G.Q., Guo, Z.T., Wu, H.B., Hao, Q.Z., 2015. Evidence of late early Miocene aridification intensification in the Xining Basin caused by the northeastern Tibetan Plateau uplift. *Glob. Planet. Chang.* 128, 31–46.
- Zhang, P., Ao, H., Dekkers, M.J., Li, Y., An, Z., 2016. Late Oligocene-Early Miocene magnetochronology of the mammalian faunas in the Lanzhou Basin-environmental changes in the NE margin of the Tibetan Plateau. *Sci Rep* 6, e38023. <http://dx.doi.org/10.31038/srep38023>.
- Zhang, H., Zhang, P., Prush, V., Zheng, D., Zheng, W., Wang, W., Liu, C., Ren, Z., 2017. Tectonic geomorphology of the Qilian Shan in the northeastern Tibetan Plateau: insights into the plateau formation processes. *Tectonophysics* 706–707, 103–115.
- Zhao, L., 2005. Variations of illite/chlorite ratio in Chinese loess sections during the last glacial and interglacial cycle: implications for monsoon reconstruction. *Geophys. Res. Lett.* 32.
- Zhao, H., Sun, Y.B., Qiang, X.K., 2017. Iron oxide characteristics of mid-Miocene Red Clay deposits on the western Chinese Loess Plateau and their paleoclimatic implications. *Palaeogeogr. Palaeoclimatol. Palaeoecol.* 468, 162–172.
- Zheng, D.W., Zhang, P.Z., Wan, J.L., Yuan, D.Y., Li, C.Y., Yin, G.M., Zhang, G.L., Wang, Z.C., Min, W., Chen, J., 2006. Rapid exhumation at similar to 8 Ma on the Liupan Shan thrust fault from apatite fission-track thermochronology: implications for growth of the northeastern Tibetan Plateau margin. *Earth Planet. Sci. Lett.* 248, 198–208.